ECS Journal of Solid State Science and Technology, **5** (6) P353-P360 (2016)
2162-8769/2016/5(6)/P353/8/$33.00 © The Electrochemical Society

Single Crystalline Germanium-Lead Formed by Laser-Induced Epitaxy

Qian Zhou,[a] Edwin Bin Leong Ong,[a] Sin Leng Lim,[b] Saumitra Vajandar,[b] Thomas Osipowicz,[b] Xiao Gong,[a] Eng Soon Tok,[b] and Yee-Chia Yeo[a,z]

[a]*Department of Electrical and Computer Engineering, National University of Singapore (NUS), Singapore*
[b]*Department of Physics, National University of Singapore (NUS), Singapore*

Single crystalline germanium-lead (GePb) is formed using pulsed laser anneal (PLA). The anneal was performed on an amorphous GePb layer (1.1 atomic percent of Pb) capped by SiO_2, Si_3N_4, or Al_2O_3 to study the impact of different capping layers on GePb formation. Among various laser fluences (300, 350, 400, 450, and 500 mJ/cm^2) used, the best GePb crystalline quality was achieved using 350 mJ/cm^2. Secondary ion mass spectrometry (SIMS) results show a final Pb composition in the GePb film after laser anneal of between 0.2 and 0.4 atomic percent, indicating a significant loss of Pb. Among the different capping layers used, Al_2O_3-capped GePb shows the highest Pb content in the GePb layer with the lowest Pb loss after PLA. The incorporation of Pb atoms in the substitutional sites of Ge lattice was confirmed by high resolution X-ray diffractometry (HRXRD) and high resolution Rutherford back scattering spectrometry (HR-RBS). The substitutionality, i.e. percentage of Pb atoms incorporated into substitutional sites of Ge lattice, is more than 70%. The anneal process leads to the formation of cavities in the GePb layer and pin holes on the surface, suggesting an out-diffusion of Pb from the GePb thin-film during laser anneal. Increasing the laser anneal fluence above 400 mJ/cm^2, however, reduces the number of cavities and pin holes but increases the surface roughness of the film.

Manuscript submitted March 29, 2016; revised manuscript received April 14, 2016. Published April 28, 2016.

Group IV alloys, such as silicon-germanium (SiGe) and silicon-carbon (Si:C), have been extensively studied for applications in nano-electronic devices, such as in SiGe heterojunction bipolar transistors,[1] and in field-effect transistors as SiGe or Si:C source/drain stressors[2] or as SiGe channel.[3] Another Group IV alloy, germanium-tin (GeSn), has also been investigated for applications such as high mobility channel metal-oxide-semiconductor field-effect transistors (MOSFETs)[4,5] and tunneling FETs (TFETs),[6] near-infrared photodetectors,[7] and Group IV lasers.[8] Going down Group IV in the periodic table, Pb is an element that may also be incorporated with other elements to form Group IV alloys. Recently, first principles calculations of the electronic properties of crystalline GePb alloys indicate that increasing the substitutional concentration of Pb would lower the Γ valley, making GePb a direct bandgap material when its Pb composition is 0.93 atomic percent or higher.[9] This is lower than the substitutional Sn composition required to achieve direct bandgap in GeSn alloys.[8] Therefore, it would be interesting to investigate the formation of single crystalline Ge-rich GePb alloys, as they may be useful for realizing semiconductor lasers or other devices that require Ge-based materials with a direct bandgap.

Solid germanium-lead (GePb) alloys can be formed by rapid quenching of liquid-phase or vapor-phase GePb.[10,11] For Ge-rich compositions, vapor quenching can retain up to 7.5 atomic percent of Pb in an amorphous Ge matrix via vapor quenching, but no detectable solubility of Pb in crystalline Ge was found in liquid-quenched GePb.GePb films can also be formed by co-sputtering of Ge and Pb,[12] or by co-evaporation,[13] but these films are not reported to be crystalline.

The phase diagram of the Pb-Ge system[14] shows no solid solubility of Pb and Ge in each other under equilibrium conditions. Ref. 15 estimated the solid solubility of Pb in Ge to be 8.9×10^{-4} atomic percent at 805°C.[15] Therefore, non-equilibrium growth techniques are preferred to form GePb alloy with Pb composition higher than its solubility limit. Chemical vapor deposition or molecular beam epitaxy of single crystalline GePb on Ge has not been reported. In our previous work, single crystalline GePb was successfully formed on the Ge substrate by using pulsed laser anneal (PLA) of an amorphous GePb alloy.[16] PLA is a non-equilibrium process that has also been used to achieve dopant activation well above its solubility limit.[17–20] While only two laser fluences (300 and 400 mJ/cm^2) and one capping layer (SiO_2) were studied in that work, it would be interesting to explore the formation of single-crystalline GePb using PLA under different capping layers. In addition, a more detailed material study is needed to investigate the impact of laser fluence on GePb formation.

In this work, the impact of different capping layers (SiO_2, Si_3N_4, and Al_2O_3) and laser fluences (300, 350, 400, 450, and 500 mJ/cm^2) on GePb formation was investigated by using various material characterization techniques, including high resolution X-ray diffractometry (HRXRD), cross-sectional TEM, atomic force microscopy (AFM), secondary ion mass spectrometry (SIMS), and RBS. We propose a mechanism to qualitatively explain the loss of Pb atoms which occurred during PLA. The evolution of the GePb morphology correlating to different laser fluences is also discussed.

Laser-Induced Epitaxy of GePb

Fig. 1a shows the process for forming crystalline GePb on Ge substrate. Lightly doped n-type Ge (100) wafers were used as the starting substrate. The substrate was cleaned by dilute hydrofluoric acid (DHF, HF:H_2O = 1:50) for 1 minute and rinsed in deionized water for three cycles. The as-cleaned substrate was immediately loaded into the magnetron sputtering system which has a base pressure of 5×10^{-7} Torr. The GePb target is a mixture of Ge and Pb. The purity of the target is above 99.999%. The Ge and Pb content in the target is 96 atomic percent and 4 atomic percent, respectively. For the sputtering process, the DC power applied on the GePb target was 30 W and the Ar gas flow rate was 25 sccm. The chamber pressure during the sputter process was 3 mTorr and the entire process was carried out at room temperature (~25°C). The GePb deposition rate was set at 1.9 nm/minute and the thicknesses of GePb deposited were 60 nm for one sample used for SIMS characterization and 40 nm for all other samples.

A cross-sectional TEM image of an as-deposited GePb sample (without capping layer) is shown in Fig. 2a. The thickness of the as-deposited GePb layer is ~40 nm. The atomic percentages of Ge and Pb measured by energy-dispersive X-ray spectroscopy (EDX) are 98.9 atomic percent and 1.1 atomic percent, respectively. High resolution TEM (HR-TEM) in Fig. 2b shows a sharp and flat GePb/Ge interface. Fast Fourier transform (FFT) analysis of a GePb region did not show long-range order in the atomic arrangement (inset in Fig. 2b), indicating that the GePb layer is amorphous. The sample was also investigated using HRXRD (PANalytical'sX'Pert PRO) with an X-ray wavelength of 0.15404 nm. In Fig. 2c, the HRXRD plot of the as-deposited GePb sample shows no additional peak near the Ge substrate peak, indicating that no single crystalline GePb was formed in the as-deposited sample. This is consistent with the HR-TEM result.

After the GePb deposition, one of three different capping layers, i.e. SiO_2, Si_3N_4, or Al_2O_3, was separately deposited on top of the sample.

[z]E-mail: yeo@ieee.org

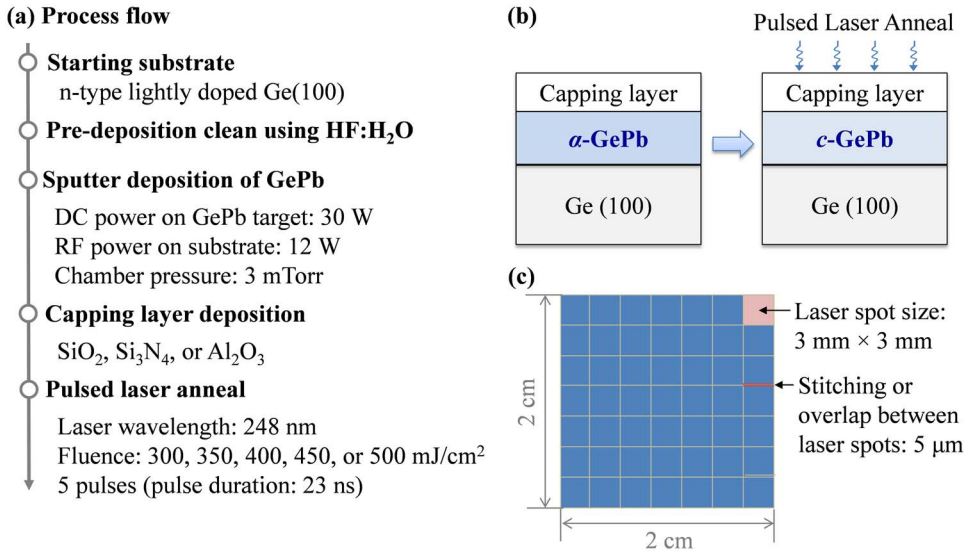

Figure 1. (a) Process flow for preparing GePb samples on Ge substrate. An amorphous layer of GePb (α-GePb, 60 nm for one sample used in SIMS characterization and 40 nm for the rest of the samples) is sputter-deposited and then capped by either SiO_2, Si_3N_4, or Al_2O_3, prior to Pulsed Laser Anneal (PLA). Each laser pulse has a fluence of 300, 350, 400, 450, or 500 mJ/cm^2. (b) PLA induces the formation of crystalline GePb (*c*-GePb). (c) Top-view illustration of sample and laser anneal process. The laser spot size is 3 mm × 3 mm. The spots are aligned side by side to cover the entire sample surface. The laser spots are stitched and the overlapping region has a width of 5 μm.

SiO_2 and Si_3N_4 were deposited at 300°C using plasma enhanced chemical vapor deposition (PECVD), while Al_2O_3 was deposited at 250°C by atomic layer deposition (ALD).

The samples were then cut into pieces each with size of 2 cm × 2 cm. A pulsed excimer laser having a wavelength of 248 nm and pulse duration of 23 ns was used for annealing to induce epitaxy (Fig. 1b). The laser was generated using a KrF source. To achieve a uniform beam energy profile, the beam was homogenized using a Beam Delivery System (BDS) and cropped using a square mask. Therefore, the final beam delivered to the samples has a square shape (with a size of 3 mm × 3 mm). The laser beam was raster scanned over the entire sample surface to complete the anneal process. Each spot was irradiated with 5 pulses and the overlap between two beam spots was 5 μm (Fig. 1c). Different laser fluences (300, 350, 400, 450, or 500 mJ/cm^2) were applied to the GePb samples. It should be noted that the laser fluence here refers to that of a single pulse fluence.

Material Characterization and Analysis

HRXRD characterization.—The crystallinity of the laser annealed samples was investigated by HRXRD at Singapore Synchrotron Light Source (SSLS).[21] The wavelength of the X-ray used is 0.15288 nm. HRXRD plots of the GePb samples with SiO_2, Si_3N_4, or Al_2O_3 cap are shown in Figs. 3a, 3b, and 3c, respectively. Each plot (same capping layer) compares the effect of different anneal fluences, and the XRD intensity is vertically displaced for easy comparison. Among the five splits in laser fluence, the fluence of 350 mJ/cm^2 per pulse gives an additional shoulder which is attributed to the presence of single crystalline GePb. The GePb shoulder has a smaller diffraction angle than the Ge substrate peak, suggesting that GePb has a larger lattice constant than Ge, due to the incorporation of Pb atoms into the substitutional sites of Ge. In order to examine the GePb more closely, the following material characterization will mainly focus on the samples that were annealed at 350 mJ/cm^2.

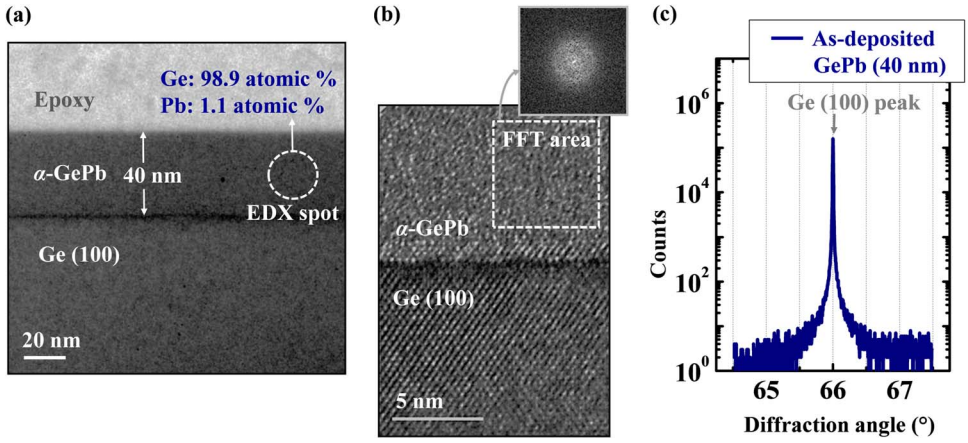

Figure 2. (a) Cross-sectional TEM image of an as-deposited GePb sample with a uniform thickness of 40 nm. EDX spectroscopy shows that the atomic percentage of as-deposited Ge and Pb is 98.9 atomic percent and 1.1 atomic percent, respectively. (b) HR-TEM image of the GePb/Ge interface. No observable oxide layer is present between Ge and GePb. No lattice fringe was found in the GePb layer. The FFT pattern in the inset indicates that GePb is amorphous. (c) HRXRD plot of the as-deposited GePb sample. Only Ge (100) peak was observed in this HRXRD plot, indicating that the GePb layer is amorphous and has no substitutional Pb.

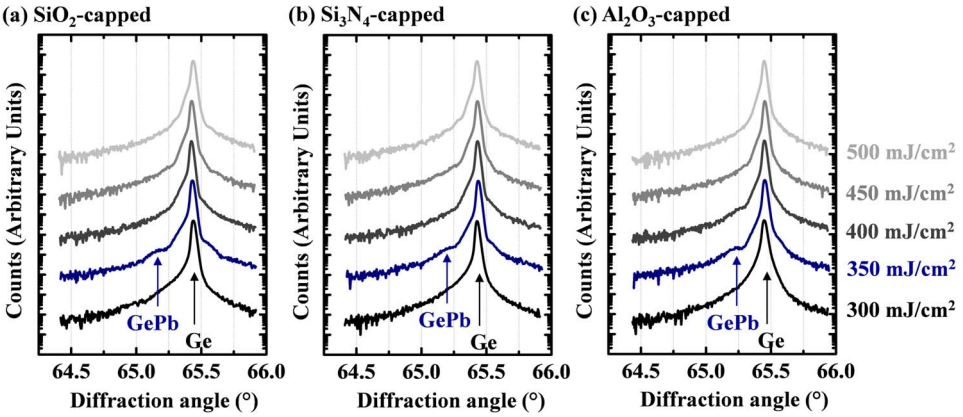

Figure 3. HRXRD plots of GePb samples covered with (a) SiO_2, (b) Si_3N_4, or (c) Al_2O_3 capping layer prior to pulsed laser anneal (PLA). Fluence of each pulse is varied from 300 to 500 mJ/cm^2. The GePb shoulder is on the left side of Ge substrate peak. This indicates the incorporation of substitutional Pb atoms into Ge and a larger lattice constant of GePb than that of Ge. Among the five laser anneal splits, PLA with fluence of 350 mJ/cm^2 gives the most obvious GePb shoulder. Thus, the best GePb crystalline quality and the highest substitutional Pb composition were obtained by this PLA condition among the fluences used in this work.

TEM and AFM analysis.—TEM analysis was performed to investigate the crystalline quality of the samples before and after the 350 mJ/cm^2 anneal. The TEM images of the GePb samples with SiO_2, Si_3N_4, or Al_2O_3 capping layer are shown in Figs. 4a, 4b, and 4c, respectively. In each sub-figure, the TEM image on the left shows the cross-section of as-capped sample before PLA, while the image in the middle (low magnification) and the image on the right (high magnification) show the sample after 350 mJ/cm^2 laser anneal. The thicknesses of SiO_2, Si_3N_4, and Al_2O_3 are 20 nm, 16 nm, and 20 nm, respectively. The GePb layers were amorphous in the as-capped samples. This suggests that the elevated temperatures used in depositing the capping layers, i.e. 300°C for SiO_2 and Si_3N_4, and 250°C for Al_2O_3, did not change the amorphous phase of the as-deposited GePb.

After the 350 mJ/cm^2 laser anneal, the GePb layer becomes crystalline. High magnification TEM images show clear lattice fringes throughout the GePb layer, including near the sample surface. This is consistent with the HRXRD results. No dislocations were observed in these regions. PLA induces a localized high temperature region near the sample surface,[20] and may have induced melting,[22,23] recrystallization, and subsequently liquid-phase epitaxy in the as-deposited GePb layer due to the relatively low melting points of Pb (327.5°C) and Ge (938.2°C).

However, as seen in the low magnification TEM images, defects were also formed within the GePb layer after laser anneal. The dark defects could be Pb precipitates due to the phase separation between Ge and Pb, while bright defects appear as cavities. Fig. 5 shows a series of cross-sectional TEM images of the samples and corresponding AFM surface morphologies. The capping layers were removed by DHF (HF:H_2O = 1:25) before TEM and AFM measurements. The TEM images show that the Al_2O_3-capped sample has the most defective GePb layer. The largest diameter of the cavities in the GePb layer is ~40 nm. The root mean square (RMS) roughness values measured from the AFM surface morphologies of the SiO_2-, Si_3N_4-, and Al_2O_3-capped samples are 4.39, 5.14, and 3.67 nm, respectively. These values are much larger than that of the as-capped samples (~0.27 nm, not shown here), indicating a significant change in surface morphology induced by PLA. Note that the Al_2O_3-capped sample has the highest pin hole density, which is consistent with the TEM observation.

SIMS characterization.—To investigate depth profile of Pb in the GePb layer, dynamic SIMS was performed for samples that were annealed at 350 mJ/cm^2 (Fig. 6). The SIMS plot was obtained from the SIMS depth profile as a function of sputter time by converting the sputter time to depth after measuring the sputter depth using a step profiler for a given sputter time. The capping layers were removed by DHF (HF:H_2O = 1:25) before measurement. Therefore, the plot only shows the Pb depth profiles within GePb/Ge layers. The Pb profile of an as-deposited 60 nm α-GePb sample without laser anneal is also shown for reference. The Pb compositions in the annealed samples are much smaller than that of the as-deposited sample, indicating a significant loss of Pb atoms in the GePb layer during PLA. In addition,

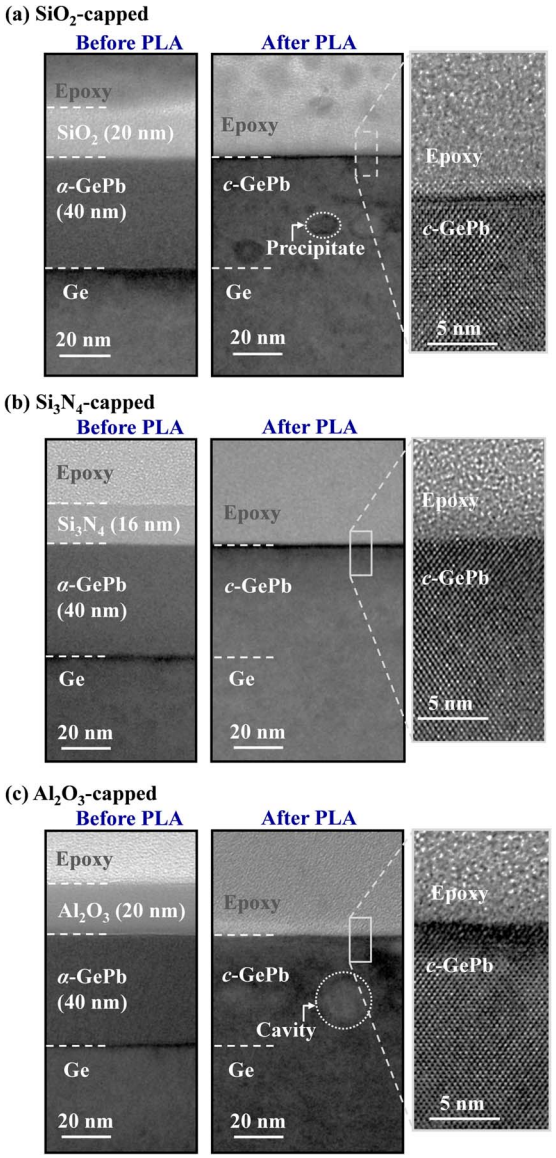

Figure 4. Cross-sectional TEM images of GePb samples with (a) SiO_2, (b) Si_3N_4, or (c) Al_2O_3 capping layer. In each sub-figure, the left TEM image shows GePb samples before PLA. The middle image (low magnification) and the right image (high magnification) show the crystalline GePb layer formed by the 350 mJ/cm^2 PLA. The capping layers of the annealed samples were removed by DHF (HF:H_2O = 1:25). It is clear that the laser anneal crystallized the α-GePb layer. Lattice fringes of the single crystalline GePb is shown in the high magnification images.

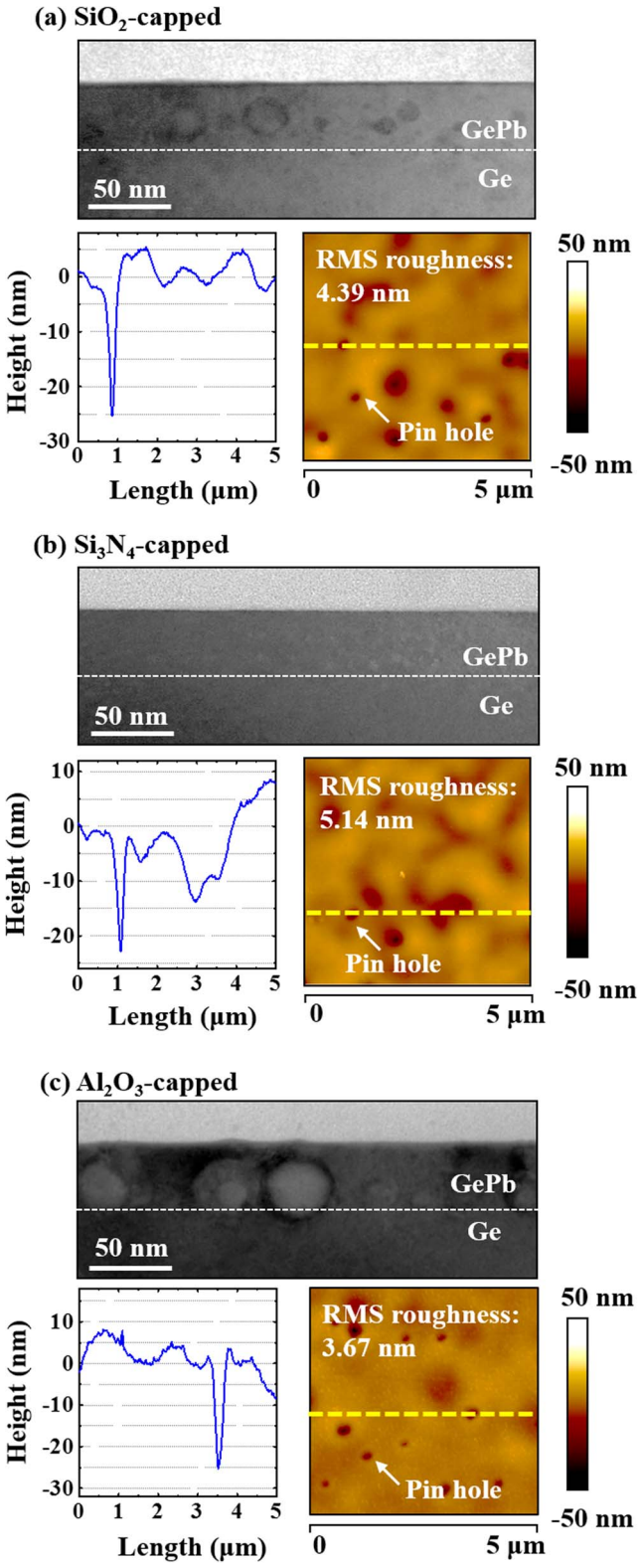

Figure 5. Low magnification XTEM images of GePb samples with (a) SiO_2, (b) Si_3N_4, or (c) Al_2O_3 capping layer. These are the same samples as those in Fig. 4. The cross-sectional TEM images show a more zoomed-out view than those in Fig. 4, thus giving a clearer view of the defect distribution. In addition, the surface morphologies of the GePb samples are shown by AFM images with a scan area of 5 μm × 5 μm. The surface profiles along the dashed lines are illustrated by the plots beside the AFM images. Surface roughening was observed in all the three samples. The pin hole densities of the SiO_2-, Si_3N_4-, and Al_2O_3-capped samples are 0.1 μm^{-2}, 0.05 μm^{-2}, and 0.5 μm^{-2}, respectively.

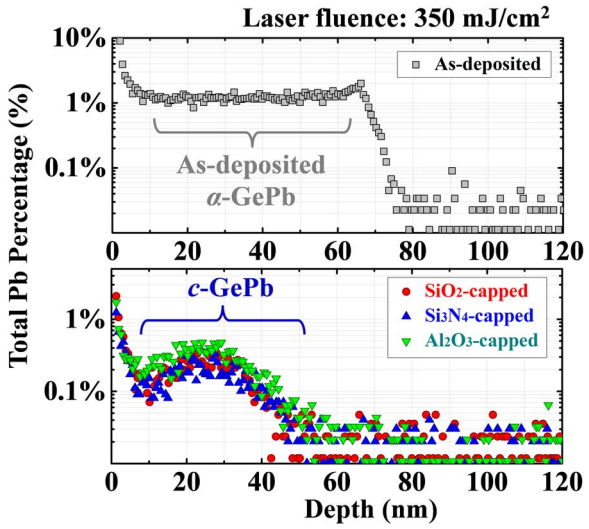

Figure 6. SIMS profiles of the as-deposited sample (upper plot) and the capped samples after 350 mJ/cm^2 PLA (lower plot). Since the capping layers were removed by DHF, only the Pb profiles within the GePb and Ge substrate are shown here. The Pb compositions in the annealed samples are much smaller than that of the as-deposited sample, indicating a significant out-diffusion of Pb atoms induced by PLA. In addition, the Al_2O_3-capped sample has the highest Pb composition in the GePb (*c*-GePb) layer.

only a slight Pb diffusion into Ge substrate was observed, indicating that the high loss of Pb should be caused by Pb out-diffusion into the capping layers. The peak concentration of Pb at a depth of ∼25 nm for all three capped samples is 0.2 ∼ 0.4 atomic percent. However, it should be noted that the Al_2O_3-capped sample has a slightly higher Pb concentration than SiO_2- and Si_3N_4-capped samples in the depth range from 5 to 50 nm. This suggests that Al_2O_3 is more efficient in reducing Pb loss than SiO_2 and Si_3N_4.

RBS characterization.—Both conventional RBS and high resolution RBS (HR-RBS) characterization were performed in this work at the Centre of Ion Beam Application, National University of Singapore.[24] Conventional RBS was used to quantify the distribution of Pb before and after laser anneal, while channeling HR-RBS used to estimate the percentage of substitutional Pb.

Fig. 7 shows the random RBS spectra of the capped samples before PLA and the reference sample (as-deposited GePb sample, without capping layer and anneal). The Pb concentration, as derived from a fit with the RBS simulation code SIMNRA[25] is ∼1.0 atomic percent, consistent with the EDX result in Fig. 2a. Moreover, the Pb backscattering peaks appear at lower energies in the capped samples than the reference sample showing that the Pb resides not at the surface of the capped samples but is retained within the GePb layer. Recall that the capping layers were either deposited at 300°C (for SiO_2 and Si_3N_4) or 250°C (for Al_2O_3). The above results, together with the results from EDX, suggest that Pb out-diffusion is not significant below 300°C.

The random-incidence RBS spectra of the laser annealed samples are shown Fig. 8. The reference sample spectrum in Fig. 7 is also included in this figure for comparison. The capping layers on the samples were removed by DHF before the RBS measurements. It was observed that the Pb peak areas in the spectra from the annealed samples are much lower than those from the reference sample, indicating lower Pb content in the annealed samples. This is attributed to the diffusion of Pb atoms into the capping layers during laser anneal. The Pb concentration retained in the GePb layer is estimated to be 0.2 ∼ 0.3 atomic percent. It should be noted that the Pb composition in Al_2O_3-capped sample is higher than that in SiO_2-capped sample, suggesting that Al_2O_3 is more efficient in preventing Pb out-diffusion than SiO_2.

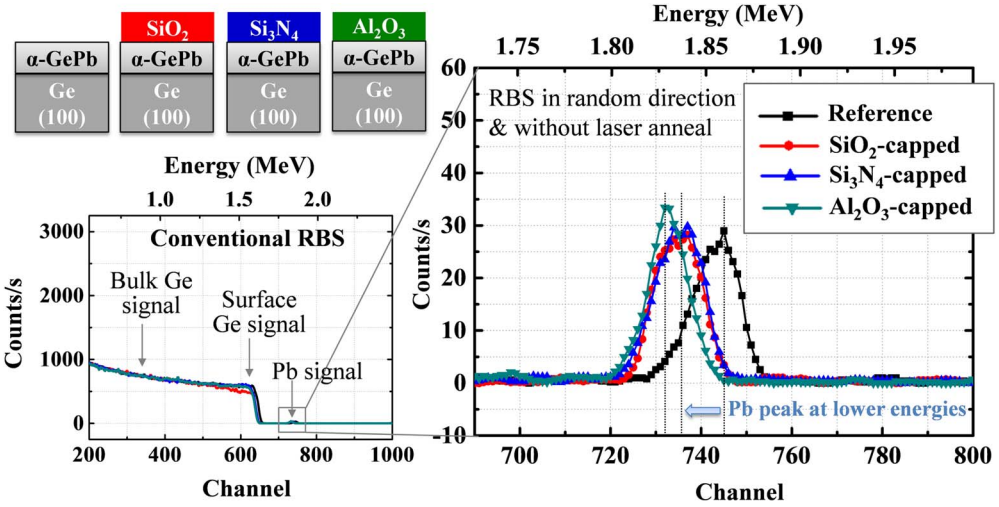

Figure 7. Conventional RBS spectra for GePb samples before PLA. The Pb composition is ∼1.0 atomic percent according to SIMNRA simulation, which is consistent with the EDX measurement. The Pb backscattering energy is smaller in the samples with capping layers (SiO_2, Si_3N_4, and Al_2O_3) as compared with the reference sample, indicating that Pb atoms are retained within the GePb layer.

Fig. 9 shows the HR-RBS spectra of the laser annealed samples. Both random and channeled spectra were measured to determine the amount of Pb on Ge lattice sites (Pb substitutionality). The zoomed-in HR-RBS spectra showing the Pb signal on the right show that the channeled Pb counts are clearly lower than the random ones, indicating that substitutional Pb. The Pb substitutionality is 70% in GePb layer of the SiO_2-capped sample, which is comparable to that in the Si_3N_4-capped sample (71%). The Pb substitutionality in the Al_2O_3-capped sample is slightly lower (63%), which could be due to morphological differences (larger cavities and/or more pin holes near the sample surface). In our previous study,[16] the Pb substitutionality values are ∼47% and ∼74% for the SiO_2-capped samples annealed at 300 and 400 mJ/cm^2, respectively. Combined with the HR-RBS results in this work, we show that a higher laser anneal fluence in the 300 to 400 mJ/cm^2 range leads to higher Pb substitutionality.

GePb surface morphology and its correlation to laser fluence.— The evolution of GePb surface morphologies of the samples with increasing laser fluence is shown in the AFM images of Fig. 10. The AFM scan area is 5 μm × 5 μm with the z-scale kept constant for all the samples. For each AFM image, the RMS roughness and surface profile along the dashed lines are also shown. The samples annealed at 300 mJ/cm^2 have the most rugged surfaces. PLA has been reported to show rapid thermal melting followed by recrystallization.[22,23] The rapid solidification is far from an equilibrium process, thus allowing a much higher concentration of Pb atoms (0.2–0.3 atomic percent) to be incorporated into the crystalline Ge-matrix as compared to the equilibrium solubility of Pb in Ge (< 0.0009 atomic percent). Ge has a much higher melting-point than Pb and is expected to recrystallize much faster than Pb. The recrystallization process is very fast and consequently, the remaining Pb atoms which are not incorporated into the Ge-matrix will be trapped beneath the surface (phase segregation) and is 'purged' to the surface before complete solidification occurs in the melt.[26] This probably forms voids in the *c*-GePb layer as shown schematically in Figure 11. When the laser fluence increases to 350 mJ/cm^2, the surface becomes less rugged and the RMS roughness is reduced for Si_3N_4- and Al_2O_3-capped samples, indicating a redistribution of surface atoms. At laser fluence of 400 mJ/cm^2, the hole number density is further reduced for all samples. However, when laser fluences are 450 mJ/cm^2 and above,

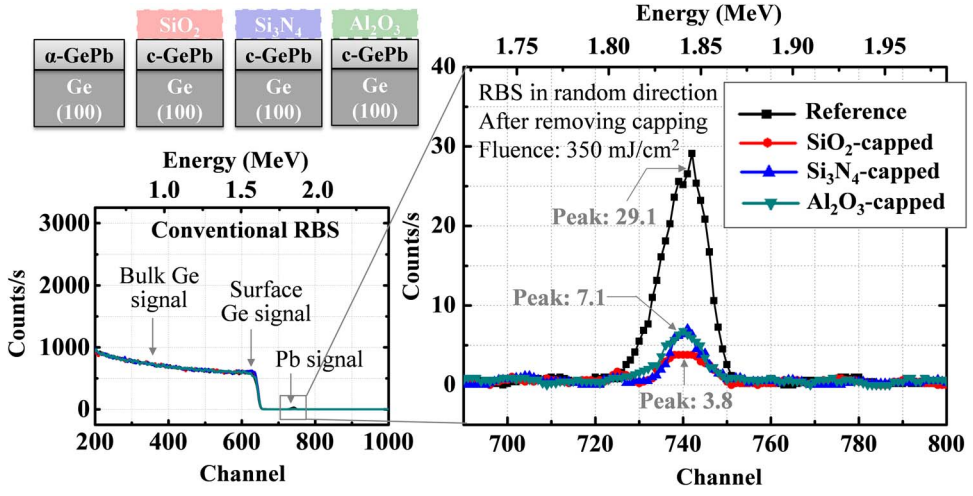

Figure 8. Conventional RBS spectra of GePb samples after 350 mJ/cm^2 PLA. The capping layers were removed by DHF ($HF:H_2O = 1:25$). The Pb counts of the annealed samples are much smaller than that of the reference sample, indicating a large amount of Pb atoms has diffused into the capping layer during PLA. The Pb composition in Al_2O_3-capped sample is higher than that in SiO_2-capped sample.

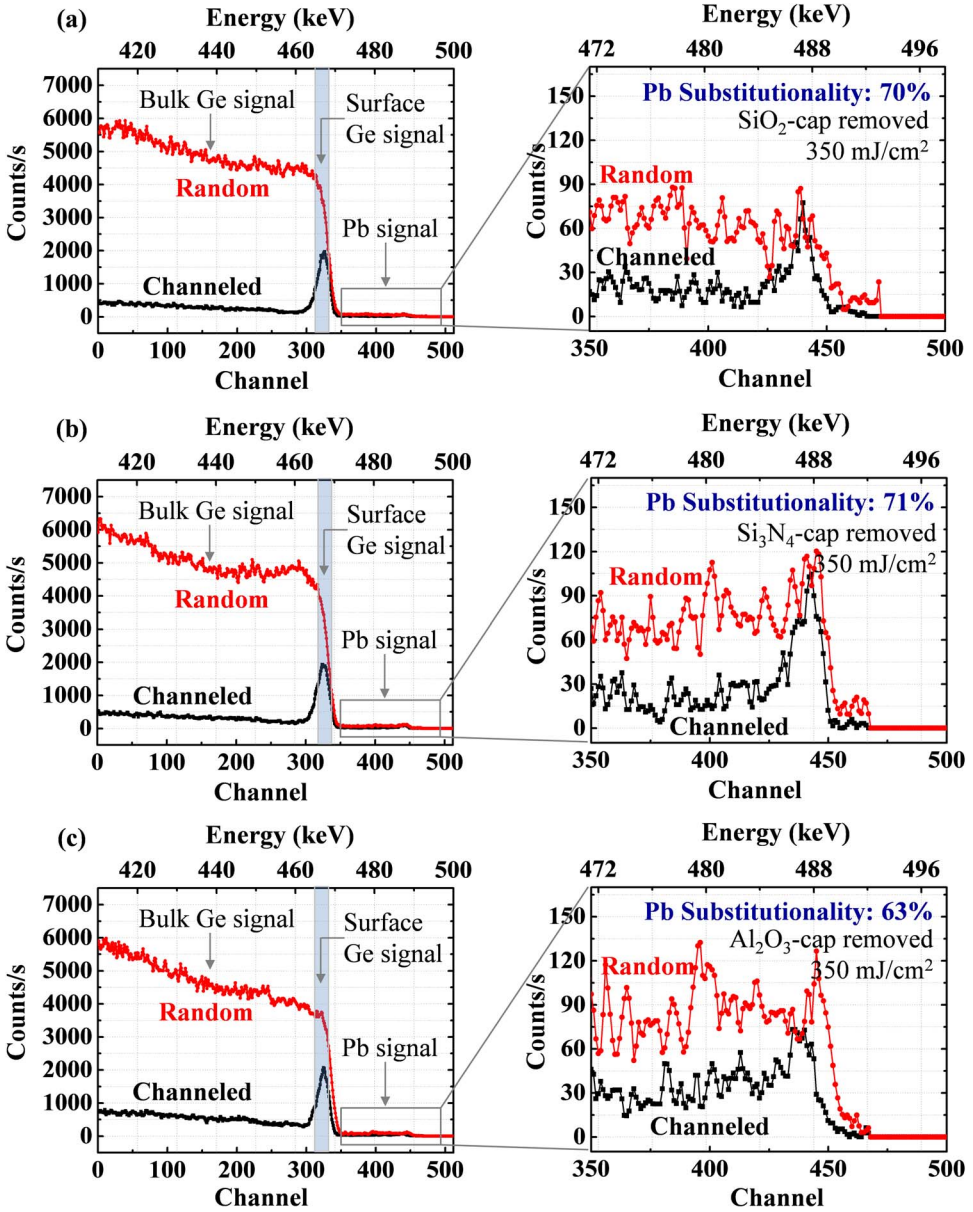

Figure 9. HR-RBS spectra of (a) SiO_2-, (b) Si_3N_4-, and (c) Al_2O_3-capped samples after 350 mJ/cm^2 PLA. The capping layers were also removed by DHF. The Pb substitutionality of the SiO_2-, Si_3N_4-, and Al_2O_3-capped samples is 70%, 71%, and 63%, respectively. Therefore, the majority of the Pb atoms in the GePb layers are incorporated into the substitutional sites after PLA.

the surface roughening starts to occur in the SiO_2- and Si_3N_4-capped samples. Surface roughening of the Al_2O_3-capped sample was not as significant as SiO_2- and Si_3N_4-capped ones, but more surface residues were observed. This effect becomes more pronounced when the laser fluence was increased to 500 mJ/cm^2, suggesting that a reaction may have occurred between Al_2O_3 and GePb.

It was reported by K. Toko et al. that annealing at lower temperature gives higher Sn composition in GeSn.[27] In pulsed laser anneal, however, the annealing temperature can vary with the laser fluence. At low laser fluence, laser anneal may not affect or change the layer composition.[28] At higher laser fluence (350 mJ/cm^2), the anneal temperature is higher and sufficient thermal energy is supplied resulting in a maximum amount of Pb incorporated into the *c*-GePb layer. This is shown by the HRXRD results in Figure 3, albeit with a significant loss of Pb. At higher laser fluence, the thermal energy supplied is higher. This will result in a higher loss of Pb from the original GePb layer as more Pb out-diffused to the surface. Consequently, the Pb composition in the Ge-Pb layer is expected to be lower.

Conclusions

The formation of crystalline GePb by PLA was studied using different laser fluences and capping layers. Among the different laser fluences used, single crystalline GePb was formed with a fluence of 350 mJ/cm^2. Cross-sectional TEM images and HRXRD analysis indicate the formation of single crystalline GePb. HR-RBS shows that the Pb substitutionality of over 70% was achieved by PLA. The final Pb composition in the GePb film is between 0.2 and 0.4 atomic percent after PLA, as confirmed by SIMS and RBS measurements. Among the different capping layers employed (i.e., SiO_2, Si_3N_4 and Al_2O_3), Al_2O_3-capped GePb sample shows the highest Pb content in the GePb layer with the lowest Pb loss after PLA. The anneal process leads to an

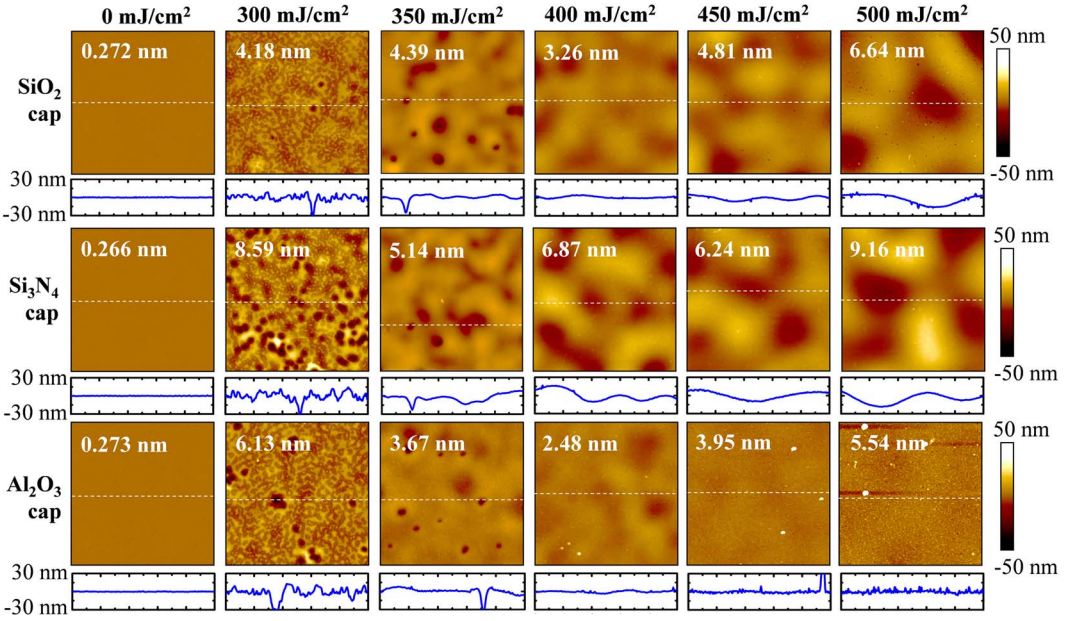

Figure 10. AFM images with a scan area of 5 μm × 5 μm show the evolution of GePb surface morphologies with increasing laser fluences. For better comparison, the z-scale is kept constant for all the samples (−50∼50 nm). The RMS roughness and the surface profile along the dashed lines are also shown in this figure. The samples annealed at 300 mJ/cm^2 have the most rugged surfaces. The RMS roughness is reduced for Si_3N_4- and Al_2O_3-capped samples when the laser fluence increases to 350 mJ/cm^2, indicating the redistribution of surface atoms. As the laser fluence increases to 400 mJ/cm^2, the hole density is reduced for all samples. However, when laser fluences are 450 mJ/cm^2 and above, the surface roughening starts to occur in the SiO_2- and Si_3N_4-capped samples. Surface roughening of the Al_2O_3-capped sample was not as significant as SiO_2- and Si_3N_4-capped ones, but more surface residues were observed. This effect becomes more pronounced when the laser fluence was increased to 500 mJ/cm^2. This suggests that a reaction may have occurred between Al_2O_3 and GePb.

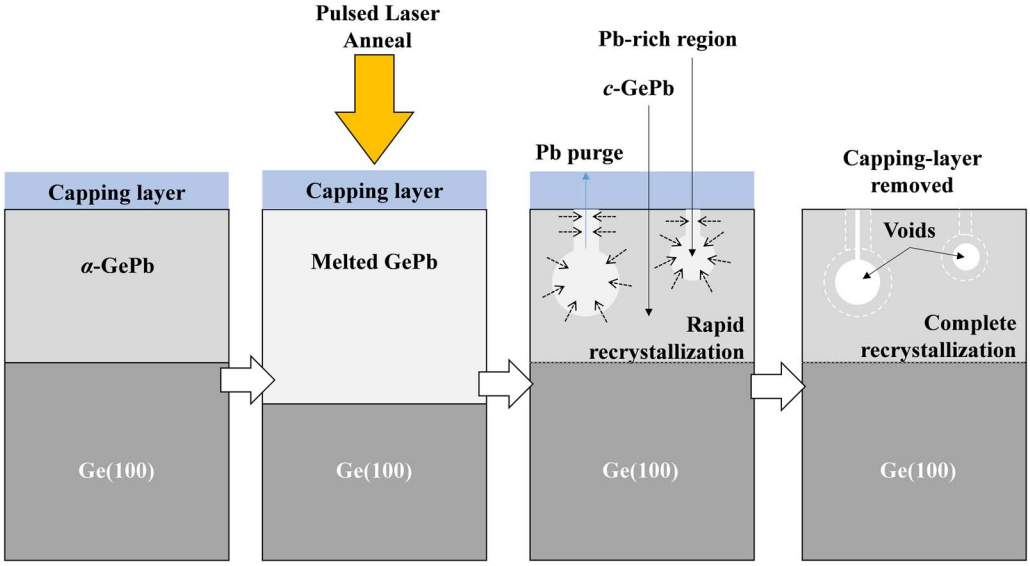

Figure 11. Schematic illustration of the pulsed laser anneal process leading to rapid melting and recrystallization of the GePb layer.

out-diffusion of Pb from the GePb thin-film. Consequently, this results in the formation of holes whose number density is reduced when the laser fluence increases above 400 mJ/cm^2, albeit with increased surface roughness.

Acknowledgments

This work was supported by Singapore National Research Foundation through the Competitive Research Program (grant No: NRF-CRP6-2010-4) and by National University of Singapore through Trailblazer grant (R-263-000-B43-733). The authors acknowledge Dr. Yang Ping at Singapore Synchrotron Light Source for the helpful discussions on HRXRD, and Arun Kumar Sesuraj for his assistance on XRD at the Department of Physics, National University of Singapore.

References

1. J. D. Cressler, *IEEE Trans. Microwave Theory and Tech.* **46**, 572 (1998).
2. Y.-C. Yeo, *Semiconductor Science and Technology* **22**, S177 (2007).
3. Y.-C. Yeo, V. Subramanian, J. Kedzierski, P. Xuan, T.-J. King, J. Bokor, and C. Hu, *IEEE Transactions on Electron Devices* **49**, 279 (2002).
4. S. Gupta, R. Chen, B. Magyari-Kope, H. Lin, B. Yang, A. Nainani, Y. Nishi, J. S. Harris, and K. C. Saraswat, *Tech. Dig. –Int. Electron Devices Meet.*, 398 (2011).
5. Y.-C. Yeo, X. Gong, M. J. H. Van Dal, G. Vellianitis, and M. Passlack, *Tech. Dig. –Int. Electron Devices Meet.*, 28 (2015).

6. Y. Yang, G. Han, P. Guo, W. Wang, X. Gong, L. Wang, K. Low, and Y.-C. Yeo, *IEEE Transactions on Electron Devices* **60**, 4048 (2013).
7. Y. Dong, W. Wang, X. Xu, X. Gong, D. Lei, Q. Zhou, Z. Xu, W. Loke, S.-F. Yoon, G. Liang, and Y.-C. Yeo, *IEEE Transactions on Electron Devices* **62**, 128 (2015).
8. S. Wirths, R. Geiger, N. Von Den Driesch, G. Mussler, T. Stoica, S. Mantl, Z. Ikonic, M. Luysberg, S. Chiussi, J. M. Hartmann, H. Sigg, J. Faist, D. Buca, and D. Grützmacher, *Nature Photonics* **9**, 88 (2015).
9. W. Huang, B. Cheng, C. Xue, and C. Li, *Physica B: Condensed Matter* **443**, 43 (2014).
10. D. Akhtar, T. C. Goel, V. D. Vankar, and K. L. Chopra, *Journal of Materials Science* **15**, 2720 (1980).
11. D. Akhtar, V. D. Vankar, T. C. Goel, and K. L. Chopra, *Scripta Metallurgica* **15**, 437 (1981).
12. A. D. Inglis, D. Landheer, D. Houghton, and R. Packwood, *Thin Solid Films* **173**, 185 (1989).
13. M. L. Rappaport and O. Entin-Wohlman, *Physical Review B* **27**, 6152 (1983).
14. R. W. Olesinski and G. J. Abbaschian, *Bulletin of Alloy Phase Diagrams* **5**, 374 (1984).
15. F. A. Trumbore, *Bell System Technical Journal* **39**, 205 (1960).
16. Q. Zhou, T. K. Chan, S. L. Lim, C. Zhan, T. Osipowicz, X. Gong, E. S. Tok, and Y.-C. Yeo, *ECS Solid State Letters* **3**, P91 (2014).
17. G. Hellings, E. Rosseel, E. Simoen, D. Radisic, D. H. Petersen, O. Hansen, P. F. Nielsen, G. Zschätzsch, A. Nazir, T. Clarysse, W. Vandervorst, T. Y. Hoffmann, and K. De Meyer, *Electrochemical and Solid-State Letters* **14**, H39 (2011).
18. S. Heo, S. Baek, D. Lee, M. Hasan, H. Jung, J. Lee, and H. Hwang, *Electrochemical and Solid-State Letters* **9**, G136 (2006).
19. Q. Zhang, J. Huang, N. Wu, G. Chen, M. Hong, L. Bera, and C. Zhu, *IEEE Electron Device Letters* **27**, 728 (2006)
20. A. T.-Y. Koh, R. T.-P. Lee, F.-Y. Liu, T.-Y. Liow, K.-M. Tan, X. Wang, G. S. Samudra, D.-Z. Chi, N. Balasubramanian, and Y.-C. Yeo, *IEEE Electron Device Letters* **29**, 464 (2008).
21. P. Yang and H. O. Moser, *Advances in Synchrotron Radiation* **1**, 105 (2008).
22. P. I. Gaiduk, S. L. Prakopyeu, V. A. Zajkov, G. D. Ivlev, and E. I. Gatskevich, *Physica B: Condensed Matter* **404**, 4708 (2009).
23. S. Stefanov , J.C. Conde , A. Benedetti, C. Serra, J. Werner, M. Oehme, J. Schulze, D. Buca, B. Holländer, S. Mantl, and S. Chiussi, *Applied Physics Letters* **100**, 104101 (2012).
24. T. Osipowicz, H. L. Seng, T. K. Chan, and B. Ho, *Nucl. Instr. and Meth. in Phys. Res. B* **249**, 915 (2006).
25. M. Mayer, SIMNRA User's Guide, Report IPP 9/113, Max-Planck-Institut für Plasmaphysik, Garching, Germany, 1997.
26. K. Sudoh, R. Hiruta, and H. Kuribayashi, *Journal of Applied Physics* **114**, 183512 (2013).
27. K. Toko, N. Oya, N. Saitoh, N. Yoshizawa, and T. Suemasu, *Applied Physics Letters* **106**, 082109 (2015).
28. L. Wang, W. Wang, Q. Zhou, J. Pan, Z. Zhang, E. S. Tok, and Y.-C. Yeo, *Journal of Applied Physics* **118**, 025701 (2015).